Journal of Materials Research and Technology 34 (2025) 2201–2211

Contents lists available at ScienceDirect

Journal of Materials Research and Technology

journal homepage: www.elsevier.com/locate/jmrt

Process enhancements and wear evaluation of directed energy deposited bronze: Implications for reducing bronze in worm gear manufacturing

Sunil Raghavendra [a], Sasan Amirabdollahian [b], Matteo Perini [b], Priyadarshini Jayashree [a], Simone Perissinotto [a], Jan Coenen [c], Matteo Benedetti [a,*]

[a] Department of Industrial Engineering, University of Trento, Trento, 38123, Italy
[b] ProM Facility, Trentino Sviluppo S.p.A, Rovereto, 38068, Italy
[c] Sicor S.R.L, Rovereto, 38068, Italy

ARTICLE INFO

Keywords:
Laser directed energy deposition (L-DED)
Bronze gear manufacturing
Additive manufacturing optimization
Wear performance evaluation

ABSTRACT

This study examines the application of Laser Directed Energy Deposition (L-DED) to reduce the use of bronze in the manufacturing of worm gears. Addressing the gap in research regarding the L-DED of bronze on steel substrates, the study refines process parameters to improve deposition quality significantly. The approach involves depositing single bronze tracks using various combinations of process parameters, followed by the analysis of cross-sections to evaluate porosity and track cross-section geometry. Building on the optimized parameters identified during single-track experiments, we achieve multi-layer depositions of 3 mm thickness. These layers are then transformed into cylindrical specimens that are subjected to rigorous wear testing in a pin-on-disc setup against a 42CrMo4V counterpart under dry sliding conditions, aimed at investigating debonding and friction characteristics. Additionally, disc-shaped specimens created with the optimized parameters are evaluated under lubricated conditions via a disc-on-disc test, accurately replicating motor gear loading scenarios. Comprehensive assessments of porosity, microstructure, and microhardness are conducted on these specimens. Finally, our findings reveal the potential of DED bronze as a groundbreaking alternative to traditional wrought bronze in gear applications, highlighting its promise for reducing bronze usage in worm gears with an enhanced wear performance.

1. Introduction

Copper and its alloys, including bronze, are extensively utilized in engineering applications owing to their superior thermal and electrical conductivity, as well as exceptional ductility. Among these applications is the production of worm wheels. Worm gearsets are integral to compact engineering systems that demand high reduction ratios, such as elevators, where they provide reliable performance in space-constrained environments [1,2]. Due to the intricate and complex tooth geometry of worm wheels, manufacturing, and assembly imperfections are common and can impede their functionality. Consequently, for heavy-duty applications, worm wheels are often made from bronze due to its ductility, which allows for better accommodation of geometric and mounting imperfections, ensuring smoother operation under demanding conditions [3]. Additionally, bronze serves as a solid lubricant and absorbs shock, mitigating wear and tear during operation. Numerous attempts [4,5] were undertaken to find alternatives to bronze in worm gearing due to its substantial copper content, a critical raw material. However, these efforts have largely yielded inconclusive results, underscoring the substantial challenge of finding alternative materials that match the unique properties and performance of bronze in these applications.

The advancement of additive manufacturing (AM) techniques over the past decade has opened promising avenues for reduced usage of critical raw materials in components without compromising their performance. This paper specifically investigates the feasibility of employing the Laser Directed Energy Deposition (L-DED) process to deposit a bronze layer of suitable thickness to significantly cut down on bronze usage while retaining the unique properties it imparts to the manufacturing of worm gears. The complex shape of worm gears leads to considering the powder feed process over the wire feed DED, despite the efficiency of the latter [6]. The L-DED can be performed by using an existing component as the substrate, offering the flexibility to not only produce new parts but also to repair and restore existing components such as turbine blades [7], tools and moulds [8], and crankshaft hub [9]

* Corresponding author.
E-mail address: matteo.benedetti@unitn.it (M. Benedetti).

https://doi.org/10.1016/j.jmrt.2024.12.242
Received 4 August 2024; Received in revised form 20 December 2024; Accepted 27 December 2024
Available online 27 December 2024

using single material or functionally graded materials [10,11]. Additionally, the development of hybrid machines that combine the L-DED process with various machining processes enables the production of components that can be directly finished to meet precise specifications [12,13]. The quality of the material deposited using the L-DED process is significantly influenced by the combination of process parameters, and the AM powder properties, such as flowability, wettability, and thermal conductivity of the material, contribute to the deposition quality [14–16].

However, it is challenging to manufacture copper and its alloys using AM processes such as L-PBF and L-DED due to its high thermal conductivity, reflectivity, and rapid oxidation. Localized thermal gradient is seen in these alloys due to rapid heat dissipation leading to problems in the melt pool and at the interface between the deposition and the substrate [17]. Also, higher laser power is required for the melting process due to their high reflectivity, which can increase the glass temperature in the laser optics beyond the permitted limit [18,19]. Nevertheless, attempts have been made to optimize the process for manufacturing Cu and its alloys due to their excellent mechanical and thermal performance. Scudino et al. [20] studied the mechanical properties of CuSn10 bronze manufactured using the L-PBF process and compared the results with cast counterparts. An enhancement in the strength and a decrease in the grain size of the microstructure was observed due to rapid cooling from the L-PBF process. Popovich et al. [21] manufactured Cu–Cr–Zr–Ti alloy using the L-PBF process with a density of 99.97 %. Columnar grains along the building direction were observed, and the strength of the specimen fabricated parallel to the building direction was higher than the specimen printed perpendicular to the building direction. Gonzalez et al. [22] cladded phosphor bronze on an alloy steel substrate using a high-power diode laser, producing finer microstructure and higher hardness coatings. Deng et al. [23] concluded that laser energy density has a non-linear relationship with mechanical properties and the deposition density for CuSn10 alloys with the best laser energy density value of 220 J/mm^2. Colopi et al. [24] focused on the limitations and the solutions for depositing Cu using a high-power single-mode fiber laser L-PBF process. A combination of high power, higher scan speed, and a base plate with lower thermal conductivity leads to a stable process. Yadav et al. [25,26] conducted a detailed study on the effect of L-DED process parameters on the deposition of pure Cu on SS30L substrate. Single tracks and multiple layers were deposited and characterized for porosity, microstructure, and hardness. Increased laser powers led to lower interlayer and intralayer porosities. A combination of equiaxed and columnar grains was observed. Yadav et al. [27] also studied the deposition of graded material with different percentages of Ni in a CuNi alloy on a Cu substrate. The laser power significantly influences track width, while the deposition height mainly depends on the scan speed. Zhang et al. [28] showed microstructure evolution from the interface to the top layer in an L-DED Cu. A noticeable dilution of the steel substrate into the deposition was observed, extending for a distance of 1.5 mm from the interface. This phenomenon indicates material intermixing at the boundary between the deposited layer and the substrate, which can impact the mechanical properties and integrity of the final product.

Additionally, very few studies have been conducted to evaluate the wear and tribological properties of additively manufactured metals. Zykova et al. [29] concluded that combining the AM process and friction stir welding of the Fe–Cu specimen led to better wear properties. Duraisamy et al. [30] studied the tribological behavior of AM stainless steel at different temperatures. Onuike et al. [31] tested L-DED manufactured Inconel 718 against an alumina ball to develop a damage zone repair strategy. Prashanth et al. [32] deduced that as-built Al–Si alloys had better wear properties compared to their annealed counterparts and cast alloys. Tombakti et al. [33] studied the effect of laser power and mode in the L-DED process of Inconel 718 on its tribological behavior, concluding that specimens manufactured with pulsed wave laser exhibit lower wear rates compared to the continuous wave. However, the wear characteristics of additive manufacturing (AM) produced materials, particularly for copper and its alloys, remain largely unexplored. Further research into how AM processes affect the wear behavior of copper alloys could provide critical insights into their potential uses and limitations, as well as guide the development of optimized manufacturing techniques to maintain or enhance their inherent qualities.

Given the critical importance of copper raw materials and the scarcity of research on the L-DED process applied to copper and its alloys, our research focuses on characterizing the L-DED process parameters for bronze and their wear performance. In our previous study, CuSn10 alloys deposited using the L-DED process on a steel substrate using a 1.5 mm nozzle were investigated. The effect of different parameters on the quality of the deposition and wear behavior under dry conditions was explored in Ref. [34]. However, for the development of the L-DED process in the production of large industrial worm gears, using a 1.5 mm nozzle has proven inefficient and unsuitable. Moreover, cast worm gears often prefer a bronze alloy with nickel due to its superior wear performance and finer grain size. Consequently, this study investigates the use of the CuSn12Ni2 alloy in the L-DED process, employing a 3 mm nozzle to achieve faster and more efficient build rates, which is particularly relevant for potential applications in worm gear production. The research examines the fine-tuning of process parameters to achieve high-quality deposition with fewer defects and enhanced adhesion in the final product. Initially, single tracks were deposited onto a steel substrate using various combinations of laser power, feed rate, and scanning speed to explore 24 distinct sets of parameters. The optimal parameters, which were determined by evaluating track bead geometry and internal porosity, established the process window for subsequent multi-layer depositions. These multi-layer depositions on a 42CrMo4V substrate were then rigorously assessed for porosity, microhardness, and microstructure. Wear tests using a Pin-on-Disc (PoD) testing apparatus under dry conditions against a 42CrMo4V counterpart are conducted to determine friction coefficients and inspect the bonding integrity between the substrate and the deposition. Additional investigations not undertaken in Ref. [34] involved fabricating cylindrical discs that were used in Disc-on-Disc (DoD) wear tests to evaluate the wear rate under lubricated conditions. This approach more accurately represents the high contact pressures experienced in the operational conditions of worm gears. Comparative assessments of the microstructure, microhardness, friction coefficients, and weight loss under lubricated conditions of these fabricated components and traditional cast bronze counterparts were conducted to evaluate the feasibility of using L-DED bronze as an alternative to cast materials.

The parameters of the multilayer deposition fine-tuned in this study permitted the deposition of bronze on the complete profile of the worm wheel, shown in Fig. 1(a). The worm wheel is subjected to a CNC machining process using a gear tooth profile cutting tool (creator tool) to obtain the final gear profile as shown in Fig. 1(b). This indicates that the process can be used as a coating technology to reduce the usage of bronze in worm wheels. The wear performance of the final gear shown in Fig. 1(b) will be investigated in the future to examine the efficiency of the L-DED process against the material performance. Eventually, a life cycle analysis of the process will be carried out to complete the study and provide a production-ready component.

2. Materials and methods

2.1. Materials

The CuSn12Ni2 air-atomized bronze powder, with particle sizes ranging from 45 to 150 μm, was procured from Linbraze S.r.l. The SEM and EDXS analyses were performed to obtain the morphology and chemical composition of the powders, respectively. The morphology shown in Fig. 2(a) indicates spherical and elongated particles attached to satellite particles. Fig. 2(b) shows the cross-sections of the powder, indicating very few internal pores in the powder particles. The chemical composition of the powders from the EDXs analysis is tabulated in

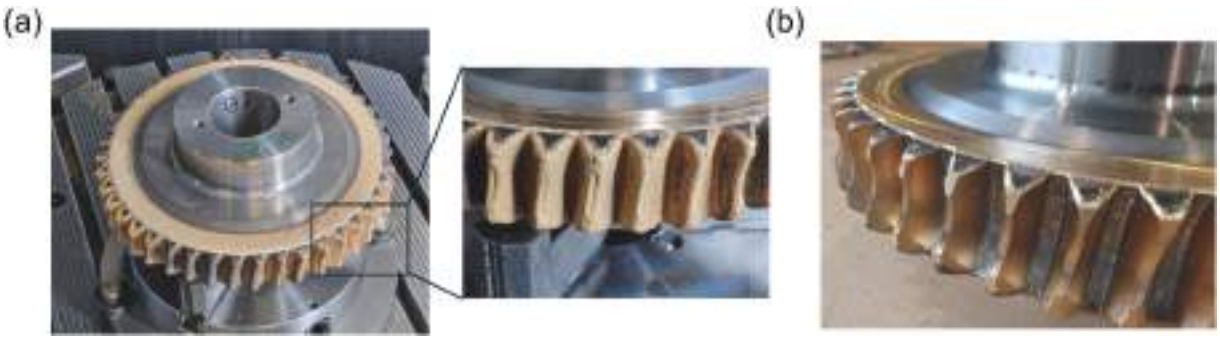

Fig. 1. Worm gear deposited with bronze alloy deposited via L-DED (a) after the deposition process (b) after machining process post-deposition.

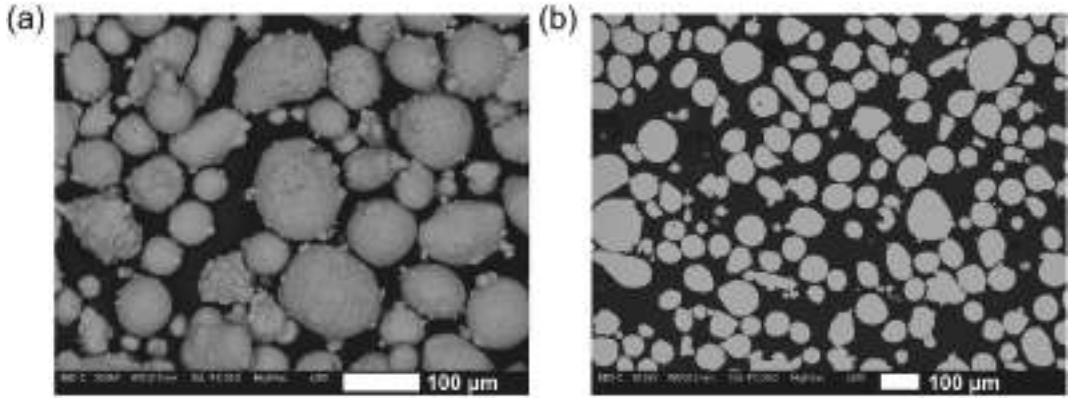

Fig. 2. SEM micrographs of bronze powders (a) powder morphology (b) cross-section of powder particles.

Table 1
Chemical composition of bronze powder.

Element	Copper (Cu)	Tin (Sn)	Nickle (Ni)
Weight percentage (%)	87.74 ± 0.12	10.56 ± 0.14	1.69 ± 0.02

Table 1.

2.2. L-DED process optimization

For the L-DED process of the bronze, a Lasertec 65 DMG MORI machine was used. This machine employed a laserline diode with a maximum laser power of 2500 W, a 3 mm coaxial nozzle, and argon carrier gas. In this study, the deposition process was fine-tined in two stages. The first stage involved the deposition of single tracks to determine the optimal parameters for the second stage, consisting of multiple-layer depositions. More details can be found in Ref. [35]. The optimal parameters from the multiple-layer deposition were used to produce cylindrical specimens for the PoD test and discs for the DoD test.

Single tracks of bronze powder were deposited on a C45 substrate, as shown in Fig. 3(a), for a length of 30 mm. A total of 24 process parameters were used by combining the laser power, scanning speed, and feed rate for the deposition process, as indicated in Table 2. The cross-section of the tracks was analyzed to study the effect of the process parameters on the porosity and the geometry of the deposited track. The aspect ratio of the bead is the ratio of track width to height, which determines the overlap and thickness of the deposition while depositing multiple layers.

The single-track deposition results in Section 3.1 laid the groundwork for depositing multiple layers on a 42CrMo4V substrate to achieve a final thickness of about 3 mm. Overlapping tracks formed a 30 mm × 25 mm rectangular deposit. Five layers were stacked to reach the desired thickness, with process parameters in Tables 3 and 4. The deposition process, shown schematically in Fig. 3(b), used a bi-directional double pass pattern, rotating each layer's direction by 90° for structural integrity. For specimens A and B, laser power was reduced by 100 W per layer to optimize energy input and minimize defects. Specimens A and C used a reduced carrier gas flow rate of 4.5 L/min for better deposition stability and quality, as detailed in Table 4. Post-deposition, cross-sections were characterized for material properties and integrity, and cylindrical pins were extracted for PoD wear testing to analyze wear characteristics.

For the DoD tests, disc-like specimens were fabricated using the parameters that demonstrated the lowest porosity levels in the multi-layer deposition process. Two specific laser power settings from L-DED, detailed in Table 5, were utilized, while the remaining parameters remained consistent with those listed in Table 3. The deposition technique for these specimens differed from that used in the multi-layer process; notably, the substrate was rotated during deposition to maintain the same scanning speed as in the multi-layer process, enhancing uniformity and consistency across the tests, as shown in Fig. 3(c). The specimens were machined to obtain discs of 24 mm outer diameters, 16 mm inner diameters, and 10 mm thickness.

2.3. Characterization

To understand how the parameters of the L-DED process affect porosity, cross-sections of single-track and multi-layer depositions were analyzed. The specimens were cut, mounted, and polished using silicon carbide abrasive papers (grit sizes 500 to 4000) and diamond suspension solutions (3 μm and 1 μm). Images were captured with a light optical microscope (LOM) and a stereomicroscope and then analyzed with ImageJ® software to evaluate porosity using the formula in Equation (1) [34,35].

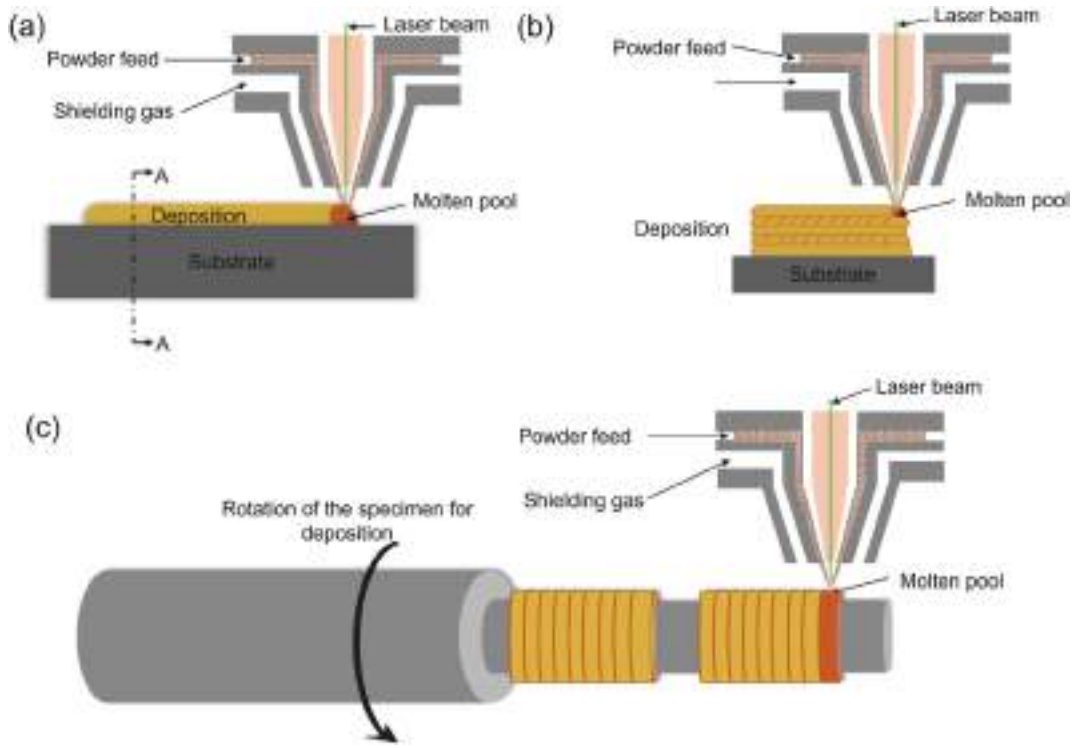

Fig. 3. Schematic representation of (a) L-DED process (b) deposition of multiple layers parameters (c) deposition on the cylindrical bar to produce discs.

Table 2
L-DED process parameters for single-track deposition.

Parameter	Unit	Value
Spot diameter	mm	3
Stand-off distance	mm	13
Laser power	Watt	1000, 1400, 1600, 1800, 2000, 2200
Scanning speed	mm/min	600, 800
Feed rate	g/min	6,8
Carrier gas flow rate	L/min	6

Table 3
Constant parameters for multi-layer deposition.

Parameter	Unit	Value
Spot diameter	mm	3
Stand-off distance	mm	13
Scanning speed	mm/min	800
Feed rate	g/min	8
Overlap	%	40

Table 4
Layerwise laser power variation for multi-layer deposition.

Specimen	Carrier gas flow rate (L/min)	Laser power (W)				
		Layer 1	Layer 2	Layer 3	Layer 4	Layer 5
A	4.5	2000	1900	1800	1700	1700
B	6	2000	1900	1800	1700	1700
C	4.5	2000	2000	2000	2000	2000
D	6	2000	2000	2000	2000	2000

Table 5
Layer wise laser power variation for deposition on a cylindrical substrate.

Specimen	Laser power (W)				
	Layer 1	Layer 2	Layer 3	Layer 4	Layer 5
Decreasing Laser	2000	1900	1800	1700	1700
Constant Laser	2000	2000	2000	2000	2000

$$Porosity = \frac{\sum Area\ of\ pores}{Total\ area} \times 100 \quad (1)$$

Microstructure analysis on cross-sections of multi-layer specimens, discs, and the wrought CuSn specimens was revealed using iron (III) chloride etchant. The average grain size was measured using ImageJ® by calculating the number of grain boundaries present for a fixed length of measurement in multiple directions.

Multi-layer specimens underwent microhardness testing with a Future-tech FM-310 Vickers microhardness tester using a 100 gf load and a 10-s dwell time. Measurements were taken in five zones, incrementing 5 mm from the substrate, and analyzed with Alexasoft software [34,35].

2.4. Wear testing

To check the endurance of the deposition on the substrate, a Pin-on-Disc (PoD) wear test was conducted under dry conditions by applying a normal load, as shown in Fig. 4(a). The L-DED pins with diameters of 10 mm and a length of 12 mm, as shown in Fig. 4(a), were extracted from the multi-layer deposition using the EDM process. The test was conducted on a Ducom® Pin-on-Disc testing machine, using a 42CrMo4V counterpart disc with a thickness of 7 mm and a diameter of 63 mm against the pin, using the testing parameters mentioned in our previous study [35].

The Disc-on-Disc (DoD) wear tests on an Amsler A135 machine measured weight loss under lubricated conditions, as shown in Fig. 4(b) for two specimens in each configuration. Shafts rotated at 500 RPM

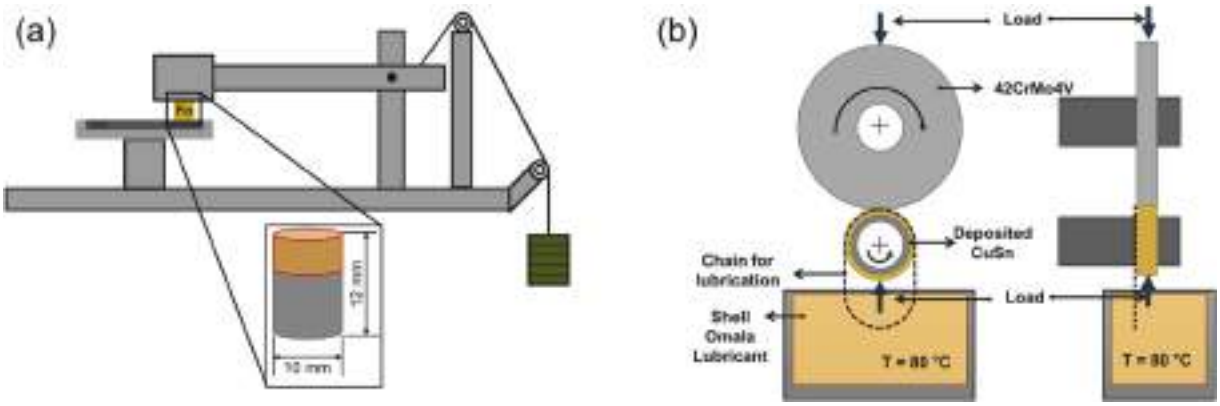

Fig. 4. Schematic representation of (a) Pin-on-disc test setup with the geometry of the pin and (b) Disc-on-Disc test setup.

Table 6
Physical characteristics of the lubricant.

Viscosity at 40 °C (mm^2/s)	Viscosity at 100 °C (mm^2/s)	Viscosity Index	Density at 15 °C (kg/m^3)
222	34.4	203	1074

(bronze) and 550 RPM (steel) to maintain a 1 m/s sliding velocity, with disc diameters of 24 mm and 56 mm and 10 mm thickness. Each disc had a surface roughness of less than 0.8 μm to minimize friction and wear. Shell Omala S4 WE220® oil with properties tabulated in Table 6, maintained at 80 ± 3 °C provided lubrication. The lubricant was transferred via a chain drive from the oil bath to the lower shaft, ensuring boundary lubrication. Radial loads were 300 MPa and 400 MPa [3] were used for a testing duration of 36 h and a total sliding distance of 129,600 m. The weight loss was measured every 6 h after the specimens were cleaned for 10 min in an ultrasonic bath with acetone. The specific weight loss and wear rate were measured with respect to the sliding distance.

3. Results and discussion

3.1. Single-track deposition

Single tracks were deposited as outlined in section 2.2. The cross-sectional images of these single tracks under various parameters are illustrated in Fig. 5. To assess the quality of these depositions, both the aspect ratio and porosity were analyzed using the optical microscope images obtained. These analyses were critical in defining the process window necessary for the successful deposition of multiple layers. The primary factors influencing the deposition height were the laser power and the amount of powder supplied. The images in Fig. 5 demonstrate that the deposition height and the circularity of the bead increase as the feed rate is adjusted upwards from 6 to 8 g/min. Moreover, for a constant feed rate, an increase in the scanning speed results in a decrease in track height. This reduction is attributed to the decreased exposure time of the material to the laser, effectively reducing the laser power per unit time, which impacts the melting and subsequent deposition processes [25]. On the contrary, the track width decreased with an increase in scanning speed for a constant feed rate and increased with an increase in the feed rate for a given scanning speed. Overall, from Fig. 6(a), an increase in the laser power increased the aspect ratio of the deposition.

According to Paul et al. [36], aspect ratio values > 5 are beneficial

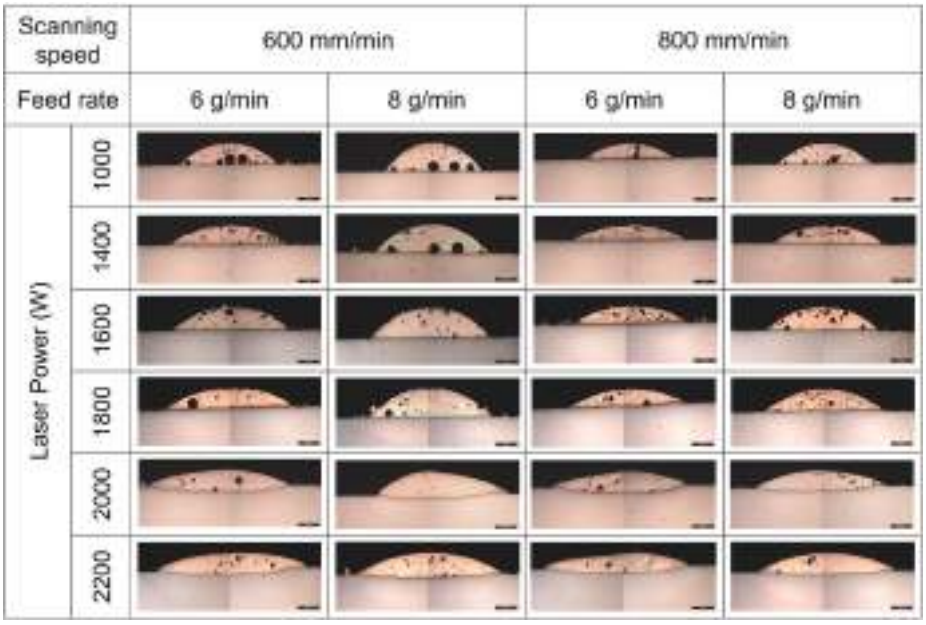

Fig. 5. Transverse cross-section of single track deposited using different process parameters.

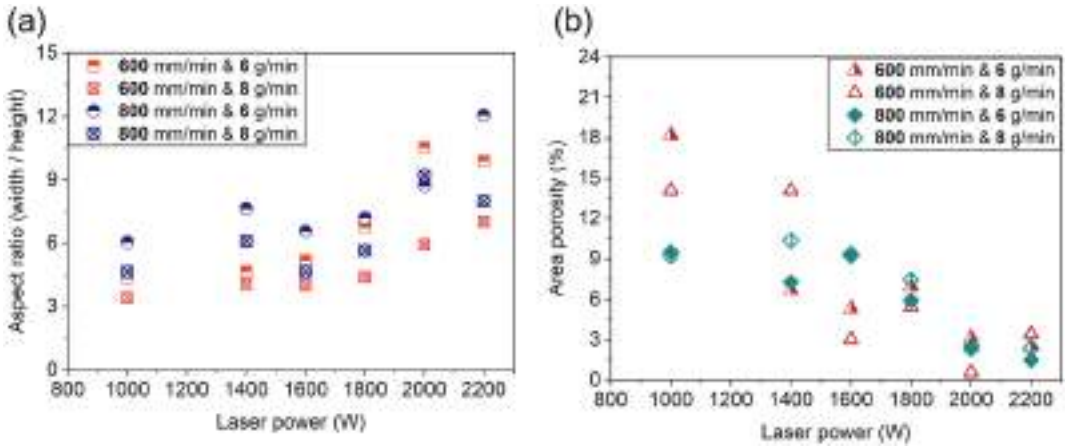

Fig. 6. Variation of (a) aspect ratio (b) area porosity for single tracks with respect to laser power. More details about process parameters fine-tuning can be found in Ref. [35].

for multi-track and multi-layer deposition to avoid inter-run porosity. Also, Yadav et al. [25] considered single-track deposition parameters that yielded aspect ratio values > 5 for multiple-layer deposition. Hence, in the current study, aspect ratio values > 5 and < 10 were considered for selecting the process window for multi-layer deposition in the next stage.

Additionally, the area porosity of the cross-section is shown in Fig. 6 (b), indicating a decrease in the porosity values with increased laser power. This correlation is attributed to the complete fusion of the deposited powder with increased laser energy. Mainly spherical pores were observed in the specimens that arise due to the gas entrapment during the deposition process. For lower laser powers, larger pores were observed closer to the substrate. Also, with an increase in the laser power, a dilution depth is seen between bronze and the substrate at a higher laser power of 2000 and 2200 W. Especially for a lower feed rate of 6 g/min and increased scanning speed, the diffusion of the substrate material into the deposition is prominent due to the increased melt pool turbulence. Therefore, based on the aspect ratio, porosity, geometrical symmetry, and diffusion on the single-track bead, a laser power of 2000 W, feed rate of 8 g/min, and a scanning speed of 800 mm/min is considered for the multi-layer deposition in the next stage. The results from the wide range of parameters considered in the study indicate that the process window for copper alloys is narrow and the required laser power is high due to the reflectivity of copper making the deposition process challenging.

3.2. Multiple layer deposition

Five layers of bronze were deposited on a 42CrMo4V substrate using four distinct parameters. The cross-sectional view of each specimen's deposition is depicted in Fig. 7. The porosity defects observed, primarily circular pores, are typically a result of gas entrapment during the deposition process. Notably, these pores are predominantly concentrated near the interface in specimens A and C, which were deposited using a lower carrier gas flow rate of 4.5 L/min. In contrast, specimens B and D were deposited with a higher carrier gas flow rate of 6 L/min. This adjustment in the carrier gas flow rate resulted in the first layer of deposition integrating more effectively with the substrate, thus forming a layer that exhibited minimal porosity. This phenomenon of substrate dilution into the deposition helped in achieving a more uniform and denser layer. The overall area porosity for the cross-sections is quantitatively analyzed and presented in Fig. 8(a). Among the specimens, the highest porosity level was recorded for specimen A, which was deposited with decreasing laser power and a lower flow rate of carrier gas. The lowest porosity, measuring just 0.35%, was observed in specimen D. Furthermore, the strategy of modulating laser power by either decreasing or maintaining it constant between layers has a significant impact on porosity outcomes. Specimens B and D, which employed a strategy of constant laser power throughout the deposition process, resulted in higher-density depositions.

The microhardness profile with respect to the thickness of the deposition is reported in Fig. 8(b). The overall hardness of the material is higher than the hardness values of the wrought specimens. A slightly higher hardness was observed closer to the substrate for specimens B and D due to the presence of Fe particles from the dilution of the substrate [37]. However, in the mid-section of the deposition, the average hardness value varies between 130 and 150 HV. Higher hardness values were reported closer to the top surface of the deposition, with values ranging between 160 and 230 HV [35]. This increased hardness is due to the rapid cooling between the heat-accumulated deposition and the

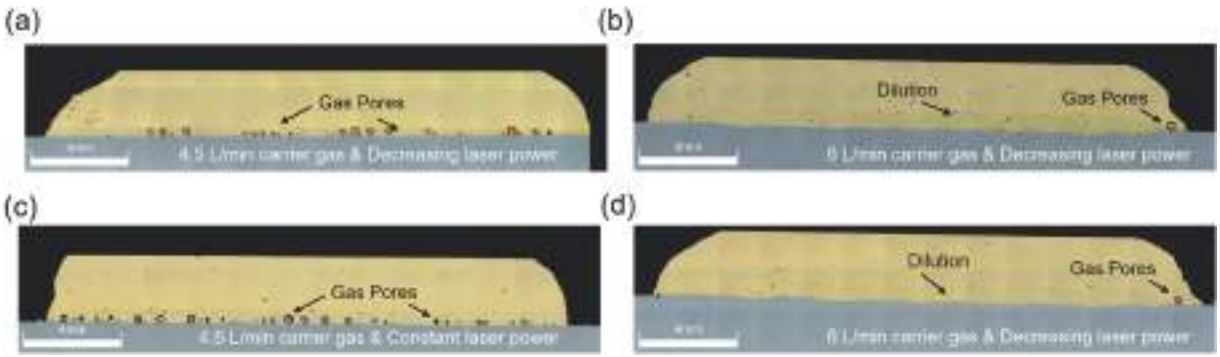

Fig. 7. Cross-section of multi-layer deposition (a) specimen A, (b) specimen B, (c) specimen C, and (d) specimen D. More details can be found in Ref. [35].

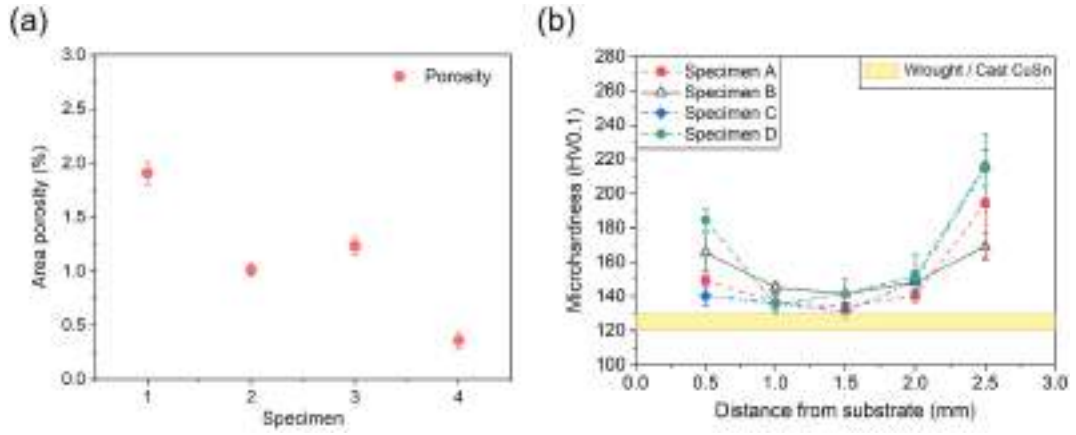

Fig. 8. (a) Area porosity of multi-layer cross-section (b) microhardness profile along the thickness of the deposition. More details can be found in Ref. [35].

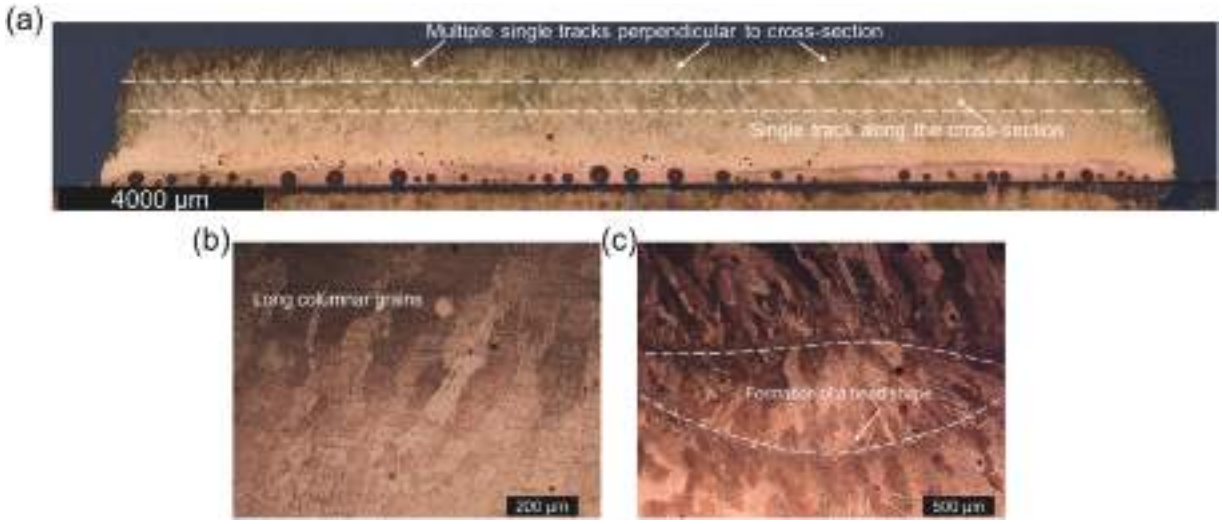

Fig. 9. (a) Microstructure of multi-layer cross-section of specimen C (b) columnar microstructure elongated along the building direction (c) deposition track boundary.

atmosphere. Also, the highest hardness in the top surface was seen for specimens C and D, which used a constant laser power due to the higher heat accumulation compared to the decreasing laser power specimens [16].

The microstructure analysis of the cross-sections revealed distinct characteristics in the L-DED specimens compared to traditional wrought specimens. In specimen C, as shown in Fig. 9(a), the complete cross-section displayed the presence of columnar grains, which contrasts sharply with the dendritic microstructure typically observed in wrought specimens, depicted in Fig. 10(c). Within the structure of specimen C, different orientations of the deposited tracks can be seen. The topmost layers display tracks that are perpendicular to the cross-section, while the layer beneath, as indicated by a dashed line in Fig. 9(a), shows tracks that are parallel. This orientation is significant as it influences the grain structure and the mechanical properties of the deposited material. A closer examination in Fig. 9(b) provides a magnified view of the columnar grains in specimen C. These grains are elongated along the building direction, a typical characteristic observed in L-DED specimens due to the directional cooling and solidification patterns during the deposition process. Furthermore, Fig. 9(c) illustrates the formation of

Fig. 10. Comparison of microstructure in (a) multilayer deposition (b) equiaxed grains in disc specimen cross-section (c) dendritic microstructure in wrought CuSn.

the bead shape from the deposition tracks that are perpendicular to the cross-section. The boundary of the bead shape is composed of smaller grains in the boundaries due to the remelting of the material [38]. A similar microstructure was observed by Yadav et al. [25,27] with columnar grain growth along the building direction for pure Cu deposited on a steel substrate.

The elongated microstructure of the multilayer specimens and the equiaxed microstructure of the disc cross-section are compared with the wrought microstructure in Fig. 10. A clear difference is seen between the DED and the wrought specimens. In the case of the disc cross-section shown in Fig. 10(b), the microstructure can be attributed to the simultaneous rotation of the substrate during the deposition process. The grain size of the three different microstructures is calculated as mentioned in section 2. The elongated grains in the multiple layer deposition (Fig. 10(a)) had an average grain size of 0.32 ± 0.12 mm along the length of the grain and 0.1 ± 0.02 mm along their width. The equiaxed grains in the disc cross-section indicated an average grain size of 0.035 ± 0.006. While the wrought specimens had the highest grain size of 0.37 ± 0.12 mm. The change in the microstructure to columnar and equiaxed is attributed to the rapid cooling and the thermal gradient in the L-DED process. The occurrence of equiaxed microstructures is consistent with findings reported for other copper alloys manufactured using AM processes, such as L-PBF [39,40] and L-DED [34,41].

3.3. Wear testing

3.3.1. Pin – on – disc

PoD tests were conducted under dry sliding conditions to compare the friction coefficient and check the endurance of the bonding between the deposition and the substrate. The variation of the friction coefficient is shown in Fig. 11(a). An initial run-in period of approximately 10 min is required to stabilize the curve and generate complete contact between the pin and disc. The average friction coefficient is obtained from the stabilized part of the curve, as shown. The average friction coefficient of the specimens is reported in Fig. 11(b). The values vary between 0.52 and 0.6 for the L-DED specimens, comparable with the wrought bronze specimens [35]. Similar friction coefficient values for CuSn10 alloys manufactured using the L-DED process and tested against a low-carbon steel counterpart were reported in our previous study [34]. The values align with the friction coefficient expected between a Copper and steel pairing [42]. Wei et al. [43] tested a GCr15 steel ball against a forged tin-bronze counter face with a hardness value between 250 and 300 HV and reported friction coefficient values between 0.8 and 0.9. Given that the multi-layer deposition underwent machining to achieve the specific dimensions needed for the pins, the hardness values near the contact surface, recorded between 140 and 150 HV, are substantiated by measurements taken at a distance of 2 mm from the substrate, as depicted in Fig. 8(b). These hardness values, considering the specific characteristics of the counterpart material and the loading conditions applied during testing, are reasonable and align with expectations for such a manufacturing process. Moreover, the absence of debonding between the deposited layer and the substrate is a critical observation, indicating strong adhesion at the interface. This result suggests that the deposition parameters were effectively optimized to ensure a robust bond between the layers. Such strong interfacial adhesion is crucial in applications where mechanical loads and wear resistance are significant factors, underscoring the success of the deposition process used in this study.

3.3.2. Disc – on – disc

Figs. 12 and 13 detail the specific weight loss and wear rate observed during the Disc-on-Disc (DoD) tests. Notably, the initial 2 h of the test—referred to as the run-in stage—exhibit significantly higher weight loss, which then transitions into a milder wear stage characterized by reduced weight loss and wear rates. This pattern suggests effective adaptation of the surfaces to each other under the test conditions. When comparing the specific weight loss and wear rates, the results for specimens exposed to constant and decreasing laser power settings overlapped, indicating that changes in laser power did not significantly affect these outcomes. Furthermore, the lower deviation observed across multiple tests confirms the good repeatability of the tests, demonstrating the reliability of the L-DED process under these specific testing conditions. Moreover, an increase in load resulted in a rise in specific weight loss, ranging from 0.08 to 0.1 g/mm/m. However, it is crucial to note that the wrought specimens exhibited higher weight loss and wear rates than the L-DED specimens across both loading conditions.

The microhardness values of the disc cross-sections are detailed and compared with the hardness of wrought bronze in Fig. 14(a). This comparison demonstrates how the microstructural differences influenced by the additive manufacturing process affect hardness outcomes. Energy-dispersive X-ray spectroscopy (EDX) analysis was performed near the top section of the cross-section, as shown in Fig. 14(b). The composition measured at different sections revealed a notable material composition change due to the dilution process during the deposition, with the presence of approximately 2% iron and 5% carbon as shown in Table 7 compared to the original powder composition shown in Table 1. This incorporation of additional elements from the substrate into the deposited material can significantly alter its mechanical properties. Additionally, the increase in hardness observed in disc specimens compared to the multi-layer deposition, as reported in Fig. 14(a), can be attributed to the transformation in microstructure from primarily columnar grains in multi-layer deposition (Fig. 9) to a finer equiaxed grain structure in the disc cross-section (Fig. 10(b)). This finer grain size results in a denser, harder material, enhancing wear resistance. These microstructural changes, along with the specific compositional adjustments from the dilution process, collectively improve the wear performance of L-DED bronze specimens over traditional wrought specimens.

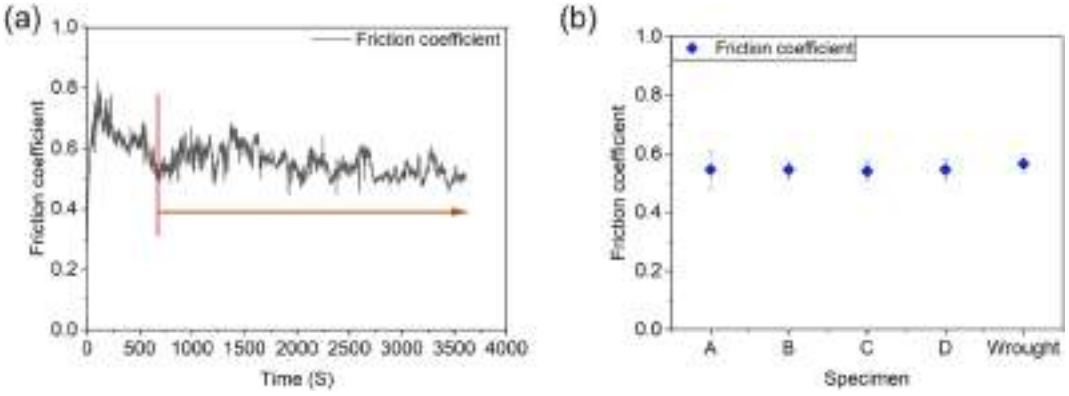

Fig. 11. (a) Representative friction coefficient variation (b) average friction coefficient values for L-DED pin compared to wrought bronze.

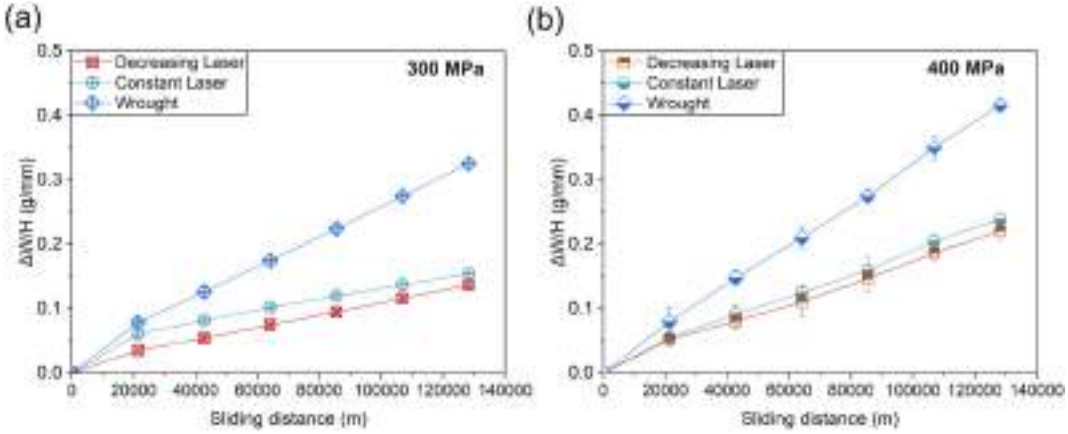

Fig. 12. Weight loss per unit width vs. sliding distance for lubricated wear test at a load of (a) 300 MPa and (b) 400 MPa.

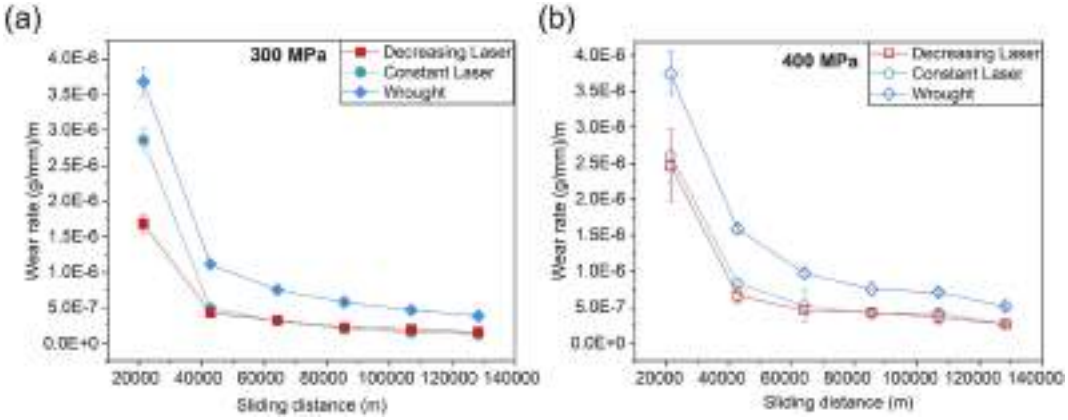

Fig. 13. Wear rate vs sliding distance for lubricated wear test at a load of (a) 300 MPa and (b) 400 MPa.

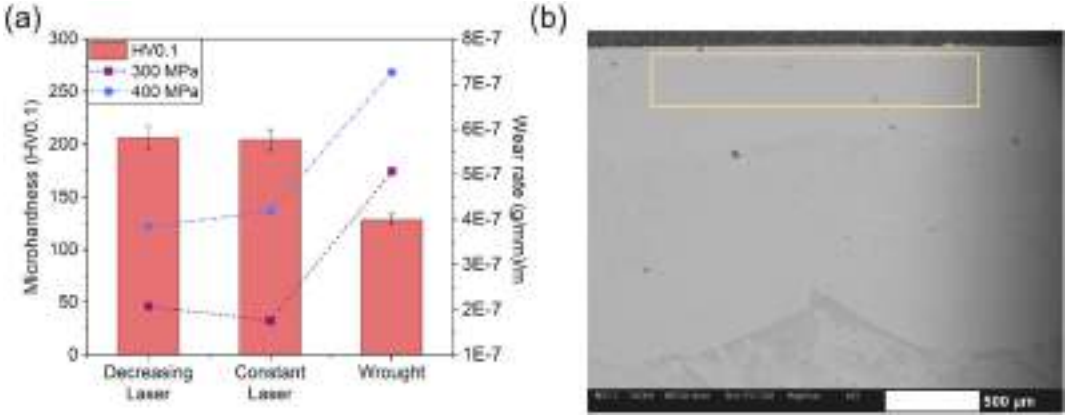

Fig. 14. (a) Comparison of microhardness values at the top surface of the cross-section for L-DED and wrought bronze discs and variation of wear rate corresponding to at a sliding distance of 100000 m (b) SEM micrograph indicating the section of the cross-section used for element composition evaluation.

Table 7
Element composition closer to the top surface of the cross-section of discs.

Specimen	Weight percentage (%)				
	Cu	Sn	Ni	C	Fe
Decreasing Laser	81.78 ± 0.04	9.65 ± 0.42	1.98 ± 0.005	4.71 ± 0.225	1.87 ± 0.25
Constant Laser	82.29 ± 0.22	9.12 ± 0.39	1.94 ± 0.04	5.27 ± 0.05	1.38 ± 0.07

4. Conclusions

The study showcased the feasibility of using Laser-Directed Energy Deposition (L-DED) for fabricating bronze worm gears, marking a significant advancement in additive manufacturing techniques.

- Single-track deposition identified optimal parameters, such as laser power exceeding 1800 W and a feed rate of 8 g/min, for achieving beads with reduced porosity and acceptable aspect ratios.

- Multi-layer deposition improvements included lower porosity and increased microhardness through carrier gas flow rates of 6 L/min and an initial laser power of 2000 W.
- Using a rotating substrate during deposition facilitated the formation of finer, equiaxed grains (average size 0.035 mm), compared to the coarser, columnar grains (average size 0.37 mm) seen in stationary substrates.
- The refined microstructure contributed to superior wear resistance, validated through Disc-on-Disc tests simulating operational conditions.
- Strong adhesion between deposited layers and substrates ensures the durability and functionality of gears for practical applications.
- L-DED manufactured bronze demonstrated better wear performance compared to traditional wrought bronze, making it a promising alternative for high-quality worm gear production.
- The results demonstrated that the process window of L-DED of bronze is narrow, making process optimization a phase crucial for successful product development.
- Further studies will focus on depositing L-DED bronze onto semi-finished steel worm gears and testing the gearsets on dedicated test benches under realistic working conditions.
- Life cycle analysis will be conducted to calculate the efficiency of the process against its performance compared to the traditional wrought gears.

Declaration of competing interest

The authors declare that they have no known competing financial interests or personal relationships that could have appeared to influence the work reported in this paper.

Acknowledgment

This work was financially supported by “Fondazione Cassa di Risparmio di Trento e Rovereto" in the framework of the project “18895-(2021.0561)-Bronze-Worm: Development of an additive manufacturing process for the efficient use of bronze in worm-wheel gearboxes”, call “Bando ricerca e sviluppo 2021/2022".

References

[1] Crosher WP. Understanding the worm gear. In: Design and application of the worm gear. ASME Press; 2002. p. 21–37.
[2] Pharkute D, Pimple V, Khandekar P, et al. Case study on design and analysis of worm gear box for elevator. Int Res J Eng Technol 2021;8:3631–9.
[3] Fontanari V, Benedetti M, Straffelini G, et al. Tribological behavior of the bronze-steel pair for worm gearing. Wear 2013;302:1520–7. https://doi.org/10.1016/j.wear.2013.01.058.
[4] Fontanari V, Benedetti M, Girardi C, Giordanino L. Investigation of the lubricated wear behavior of ductile cast iron and quenched and tempered alloy steel for possible use in worm gearing. Wear 2016;350–351:68–73. https://doi.org/10.1016/j.wear.2016.01.006.
[5] Steingröver K. Untersuchungen zu Verschleiß. Verlustgrad und Fressen bei Zylinder-Schneckengetrieben. Technische Universität München; 1993.
[6] Ahn D-G. Directed energy deposition (DED) process: state of the art. Int J Precis Eng Manuf Technol 2021;8:703–42. https://doi.org/10.1007/s40684-020-00302-7.
[7] Nowotny S, Scharek S, Beyer E, Richter K-H. Laser beam build-up welding: precision in repair, surface cladding, and direct 3D metal deposition. J Therm Spray Technol 2007;16:344–8. https://doi.org/10.1007/s11666-007-9028-5.
[8] Ren L, Panackal A, Ruan J, et al. Three dimensional die repair using a hybrid manufacturing system. 2006.
[9] Piasecki A, Bartkowski D, Młynarczyk A, et al. Laser cladding of Stellite 6 on low carbon steel for repairing components in automotive applications using disk laser. Arch Mech Technol Autom 2013;33:25–34.
[10] Bobbio LD, Otis RA, Borgonia JP, et al. Additive manufacturing of a functionally graded material from Ti-6Al-4V to Invar: experimental characterization and thermodynamic calculations. Acta Mater 2017;127:133–42. https://doi.org/10.1016/j.actamat.2016.12.070.
[11] Onuike B, Heer B, Bandyopadhyay A. Additive manufacturing of Inconel 718—copper alloy bimetallic structure using laser engineered net shaping (LENS^{TM}). Addit Manuf 2018;21:133–40. https://doi.org/10.1016/j.addma.2018.02.007.
[12] Nyamuchiwa K, Palad R, Panlican J, et al. Applied sciences recent progress in hybrid additive manufacturing of metallic materials. 2023.
[13] Dávila JL, Neto PI, Noritomi PY, et al. Hybrid manufacturing: a review of the synergy between directed energy deposition and subtractive processes. Int J Adv Manuf Technol 2020;110:3377–90. https://doi.org/10.1007/s00170-020-06062-7.
[14] Ribeiroa Kandice SB, Marianib Rtc Fábio E. Different deposition strategies strategies in direct energy deposition processes (DED). Procedia Manuf 2020;48:663–70. https://doi.org/10.1016/j.promfg.2020.05.158.
[15] Liu M, Kumar A, Bukkapatnam S, Kuttolamadom M. A review of the anomalies in directed energy deposition (DED) processes & potential solutions - part quality & defects. Procedia Manuf 2021;53:507–18. https://doi.org/10.1016/j.promfg.2021.06.093.
[16] Svetlizky D, Zheng B, Vyatskikh A, et al. Laser-based directed energy deposition (DED-LB) of advanced materials. Mater Sci Eng, A 2022;840:142967. https://doi.org/10.1016/j.msea.2022.142967.
[17] Singer F, Deisenroth DC, Hymas DM, Ohadi MM. Additively manufactured copper components and composite structures for thermal management applications. In: 2017 16th IEEE intersociety conference on thermal and thermomechanical phenomena in electronic systems (ITherm). IEEE; 2017. p. 174–83.
[18] Frigola P, Harrysson OA, Horn TJ, et al. Fabricating copper components with electron beam melting. AM&P Tech Artic 2014;172:20–4. https://doi.org/10.31399/asm.amp.2014-07.p020.
[19] El-Wardany TI, She Y, Jagdale VN, et al. Challenges in three-dimensional printing of high-conductivity copper. J Electron Packag 2018;140. https://doi.org/10.1115/1.4039974.
[20] Scudino S, Unterdörfer C, Prashanth KG, et al. Additive manufacturing of Cu-10Sn bronze. Mater Lett 2015;156:202–4. https://doi.org/10.1016/j.matlet.2015.05.076.
[21] Popovich A, Sufiiarov V, Polozov I, et al. Microstructure and mechanical properties of additive manufactured copper alloy. Mater Lett 2016;179:38–41. https://doi.org/10.1016/j.matlet.2016.05.064.
[22] Arias-González F, del Val J, Comesaña R, et al. Production of phosphor bronze coatings by laser cladding. Procedia Manuf 2017;13:177–82. https://doi.org/10.1016/j.promfg.2017.09.031.
[23] Deng C, Kang J, Feng T, et al. Study on the selective laser melting of CuSn10 powder. Materials 2018;11:1–7. https://doi.org/10.3390/ma11040614.
[24] Colopi M, Demir AG, Caprio L, Previtali B. Limits and solutions in processing pure Cu via selective laser melting using a high-power single-mode fiber laser. Int J Adv Manuf Technol 2019;104:2473–86. https://doi.org/10.1007/s00170-019-04015-3.
[25] Yadav S, Paul CP, Jinoop AN, et al. Laser directed energy deposition based additive manufacturing of copper: process development and material characterizations. J Manuf Process 2020;58:984–97. https://doi.org/10.1016/j.jmapro.2020.09.008.
[26] Yadav S, Paul CP, Rai AK, et al. Parametric studies on laser additive manufacturing of copper on stainless steel. J Micromanufacturing 2022;5:21–8. https://doi.org/10.1177/25165984211047525.
[27] Yadav S, Jinoop AN, Sinha N, et al. Parametric investigation and characterization of laser directed energy deposited copper-nickel graded layers. Int J Adv Manuf Technol 2020;108:3779–91. https://doi.org/10.1007/s00170-020-05644-9.
[28] Zhang X, Chen Y, Pan T, et al. Joining of copper and stainless steel 304L using direct metal deposition. Solid Free Fabr 2019 Proc 30th Annu Int Solid Free Fabr Symp - An Addit Manuf Conf SFF 2019;2019:388–403.
[29] Zykova A, Chumaevskii A, Vorontsov A, et al. Evolution of microstructure and properties of Fe-Cu, manufactured by electron beam additive manufacturing with subsequent friction stir processing. Mater Lett 2022;307:131023. https://doi.org/10.1016/j.matlet.2021.131023.
[30] Duraisamy R, Kumar SM, Kannan AR, et al. Tribological performance of wire arc additive manufactured 347 austenitic stainless steel under unlubricated conditions at elevated temperatures. J Manuf Process 2020;56:306–21. https://doi.org/10.1016/j.jmapro.2020.04.073.
[31] Onuike B, Bandyopadhyay A. Additive manufacturing in repair: influence of processing parameters on properties of Inconel 718. Mater Lett 2019;252:256–9. https://doi.org/10.1016/j.matlet.2019.05.114.
[32] Prashanth KG, Debalina B, Wang Z, et al. Tribological and corrosion properties of Al-12Si produced by selective laser melting. J Mater Res 2014;89:2044–54. https://doi.org/10.1557/jmr.2014.133.
[33] Tombakti IA, Adesina AY, Alharith A, et al. Effect of laser mode and power on the tribological behavior of additively manufactured Inconel 718 alloy. J Tribol 2023;145. https://doi.org/10.1115/1.4062361.
[34] Raghavendra S, Jayashree P, Rita DA, et al. Wear and material characterization of CuSn10 additively manufactured using directed energy deposition. Addit Manuf Lett 2023;6:100136. https://doi.org/10.1016/j.addlet.2023.100136.
[35] Raghavendra S, Amirabdollahian S, Perini M, et al. Development of DED process parameters for deposition of bronze and evaluation of its wear properties under dry sliding conditions. Procedia Struct Integr 2024;53:119–28. https://doi.org/10.1016/j.prostr.2024.01.015.
[36] Paul CP, Bhargava P, Kumar A, et al. Laser rapid manufacturing: technology, applications, modeling and future prospects. In: Lasers in manufacturing. John Wiley & Sons, Ltd; 2013. p. 1–67.
[37] Yao CL, Kang HS, Lee KY, et al. A study on mechanical properties of CuNi2SiCr layered on nickel-aluminum bronze via directed energy deposition. J Mater Res Technol 2022;18:5337–61. https://doi.org/10.1016/j.jmrt.2022.04.159.
[38] Liu X, Wang H, Kaufmann K, Vecchio K. Directed energy deposition of pure copper using blue laser. J Manuf Process 2023;85:314–22. https://doi.org/10.1016/j.jmapro.2022.11.064.

[39] Zhang W, Zhang B, Xiao H, Zhu H. Interfacial phenomena and microstructure of copper/steel bimetal structure produced by a new hybrid additive manufacturing process combining selective laser melting and directed energy deposition. Mater Sci Forum 2022;1054 MSF:31–6. https://doi.org/10.4028/p-vrktc3.
[40] Chen J, Yang Y, Wang D, et al. Effect of manufacturing steps on the interfacial defects of laser powder bed fusion 316L/CuSn10. Mater Lett 2021;292:129377. https://doi.org/10.1016/j.matlet.2021.129377.
[41] Zhang X, Pan T, Chen Y, et al. Journal of Materials Science & Technology Additive manufacturing of copper-stainless steel hybrid components using laser-aided directed energy deposition. J Mater Sci Technol 2021;80:100–16. https://doi.org/10.1016/j.jmst.2020.11.048.
[42] Straffelini G. Friction and. Wear: methodologies for design and control. 2015.
[43] Wei C, Niu C, Tan Y, Lei Z. Dry-sliding tribological properties of a tin–bronze alloy produced by multiaxial forging and annealing. Ind Lubric Tribol 2022;74:692–7. https://doi.org/10.1108/ILT-01-2022-0014.